Progress in Additive Manufacturing (2024) 9:461–469
https://doi.org/10.1007/s40964-023-00465-0

FULL RESEARCH ARTICLE

Auxetic behavior of 3D-printed structure made in acrylonitrile butadiene styrene and carbon fiber-reinforced polyamide

Alessandro Pellegrini[1] · **Maria Emanuela Palmieri**[1] · **Fulvio Lavecchia**[1] · **Luigi Tricarico**[1] · **Luigi Maria Galantucci**[1]

Received: 30 January 2023 / Accepted: 28 May 2023 / Published online: 6 June 2023

Abstract
Parts with an auxetic structure, which exhibit negative Poisson's ratio, can be associated with a novel class of smart materials. Such interesting property has been widely explored, over the time, for different applications, i.e., medical, automotive, robotic and aeronautic field. However, the research about the design and analysis of auxetic behavior is still on the way. In this paper, a 2D re-entrant honeycomb structure was realized using material extrusion additive manufacturing technology. Two different materials, acrylonitrile butadiene styrene and carbon fiber-reinforced polyamide were adopted. The technique of digital image correlation was implemented during the tensile test to evaluate over the time and in different areas of specimens the strain behavior of the auxetic structure for both investigated materials. The measured negative Poisson's ratio confirmed the auxetic behavior of the designed structure. The comparison between the two investigated materials showed a different trend of negative Poisson's ratio.

Keywords MEX · Additive manufacturing · Digital image correlation · Negative Poisson · ABS · Onyx

1 Introduction

Auxetic materials are a special class of materials that have Poisson's ratio (ν) with negative values compared to the conventional materials [1]. In fact, the term "auxetic" was used for the first time by Evans [2] to define the behavior of materials that exhibited a negative Poisson's ratio (NPR). They are able to expand/contract transversely while tensioned/compressed in the longitudinal direction [3]. This main characteristic enables to realize structures or materials with excellent mechanical properties. Lakes demonstrated that auxetic materials show an higher shear modulus [4], higher fracture toughness [5], a higher indentation resistance [6] and higher energy absorption [7], in particular for some application fields where these properties are requested as the aerospace, automotive and biomedical.

The NPR is due to the geometry of materials that are inspired by mineral and biological forms like α-cristobalite, silicone-dioxide polymorph [8, 9] or human spongy bone [10]. The complexity in the production of these types of structures has required the application of unconventional manufacturing technology as the additive manufacturing (AM). One of the main advantages of additive technologies is the possibility to realize, more easily, complex shapes and products with a relative low cost and flexibility, which are not either possible or cost effective to manufacture through conventional manufacturing techniques [11, 12]. Indeed, the advent and benefits from the enormous progress of AM technologies have contributed to increase the research about complex structures as the auxetic ones and their fabrication from metals and polymers even composites [13, 14] and can immensely help in the production of small and intricate parts for sophisticated applications such as sensors, soft robotics, and other similar applications [1]. However, AM technologies suffer from a strong anisotropy, in particular for parts made by powder bed fusion (PBF) [15] and by material extrusion additive manufacturing (MEX) [16]. The manufacturing defects are one of the disadvantages that influence the aspect, the quality and the mechanical performance of the printed part. Gaps between thin walls, blobs, scars on the top layer, stringing, over-extrusion, and under-extrusion, residuals of sintered powder and staircase effect for small

✉ Alessandro Pellegrini
alessandro.pellegrini@poliba.it

[1] Dipartimento di Meccanica Matematica e Management, Politecnico di Bari, Bari, Italy

features are some defects reported in literature for MEX [17, 18] and PBF [19].

Several 2D/3D auxetic structures and their different mechanism deformation [20] are studied in the open library. The 2D re-entrant type was the first example with the honeycomb based [2, 4]. The triangular based [21] and the double arrowhead [22] are other types of re-entrant-based structures. The re-entrant honeycomb-based structure showed a ν value, depending on the number of cells, in a range of $-0.40 \leq \nu < -0.10$ [3]. Chiral structure is a typical 2D honeycomb structure, having three, four, and six ligaments attached to them, which can also be divided into chiral and antichiral honeycombs according to the rotation direction. Several geometries can be considered chiral based [23, 24] and in general, the values are comprised in a range of $-1.0 \leq \nu < -0.5$.

The NPR is mainly affected by geometrical parameters such as the circumferential struct number, radius of the struct, ligament angle, and the consequent variation in the stent length, re-entrant angle, thickness of the struct [1, 25]. Literature offers several examples of works that explain how geometrical parameter can affect the deformation behavior and mechanical properties of auxetic structures. Yang et al. [19] compared two 3D auxetic structure realized in Ti–6Al–4V with different geometrical aspects as re-entrant angle and ratio between vertical length (h) and re-entrant strut (l). For large re-entrant angle as well as the h/l ratio, the negative Poisson's ratio became bigger. Liu et al. [21] compared five different auxetic structures for soft elastomeric capacitor (the re-entrant hexagonal honeycomb, re-entrant triangular-shaped honeycomb, re-entrant star system, chiral truss, and zigzag triangular network patterns) with the aim to understand which kind of structure enhance sensing properties. Wan et al. [25] proposed a theoretical approach for re-entrant cell subjected at large deformation and they showed that geometrical aspects as the h/l and re-entrant angle have a very significant effect on the magnitude of the Poisson's ratio. Fu et al. [26] proposed a novel chiral 3D isotropic structure, studying the relation between equivalent elastic parameter and geometric variables. Wang et al. [27] paid attention on the influence of strut thickness variation on the deformation mechanism of the structure. Wang et al. [28] observed for the Poisson's ratio of a composite auxetic 3D re-entrant structure a parabolically depends on the re-entrant angle with a marked auxetic behavior than a steel structure used as comparison. Moreover, increasing the angle from 35° to 70°, the NPR varied from about -1.2 to -0.5.

The experimental evaluation of Poisson's ratio were generally carried out with image-based methods by adopting a digital image correlation (DIC) technique [18, 29, 30] which requires a monitoring in-process or an image processing software through a post-processing analysis [13, 23, 31].

Meeusen et al. [13] investigated five different geometries of re-entrant honeycombs and tested four structures for kinesiology tapes application. The determination of the Poisson's ratio was derived with a post-processing method using the photos acquired. Riva et al. [23], using a post-processing method, evaluated the NPR of chiral and re-entrant honeycomb structure realized with two different technologies of AM, as fused filament fabrication (FFF) and stereolithography (SLA), processing three different materials. The epoxy-resin structures showed a more auxeticity than the other two thermoplastics. Bronder et al. [29] investigated, using the DIC technique, the mechanical characteristics of the two auxetic models. Authors concluded how thin struts lead to relatively high Poisson's ratios but poor energy absorption capacity, whereas thick struts will increase the energy absorption capacity but lower the auxetic effect. Zhang et al. [30], using the experimental test with DIC and finite element analysis, carried out the mechanical properties of 3D-printed auxetic structures realized in epoxy-resin and stainless-steel. Authors found how during the entire test, the auxetic behavior is respected up to a certain value of strain, beyond the Poisson's ratio became positive. Ling et al. [31] explored the Poisson's ratio for different metamaterials at large magnitude.

In the present work, a 2D re-entrant honeycomb cell was designed and printed using the material extrusion additive manufacturing technology (MEX). Two different materials were considered and compared. One is the most common 3D printing material, acrylonitrile butadiene styrene (ABS); the second is a carbon fiber-reinforced polymer (CFRP). This is a proprietary material of Markforged Inc. called Onyx™, polyamide-6 (PA6) with micro carbon fiber chopped. Onyx has about twice the elongation at break and about three times the impact strength of ABS [32, 33]. These characteristics make it interesting for automotive applications and safety devices, indeed it is an excellent material for absorbing energy during deformation.

DIC system allowed to monitor during the entire tensile test, the deformations along both axial and transversal direction. The analysis was carried out by measuring the deformation of the specimen along three lines in transversal direction (near the mobile grip, in the middle of the specimen and near the fixed grip) and along one line in axial direction (in the middle of specimen). This analysis allowed to derive the correlation between the Poisson's ratio and axial strain detecting exactly the moment in which the structure exhibits an auxetic behavior. Moreover, DIC system was exploited to observe the influence of the investigated zone of the specimen on the value of Poisson's ratio and transversal strain.

2 Materials and methods

2.1 Cell design

Using the commercial software nTopology (nTopology Inc.), a 2D re-entrant honeycomb cell was designed. As discussed in Sect. 1, the Poisson's ratio is affected by geometrical aspects, in particular for the design of the cell are fundamental: horizontal length (L), vertical length of the cell (h), strut thickness (t), re-entrant strut (l) and re-entrant angle (θ). The L and t parameters are set equal to 5 mm and 0.8 mm, respectively, to obtain a sufficient printing quality and respecting the technological limits of the process. Consequently, importing the mesh on GOM Inspect software, the other parameters were derived: $h = 3.63$ mm, $l = 2.69$ mm and $\theta = 68.20°$. In Fig. 1a, a sketch of the 2D re-entrant cell is shown. In Fig. 1b, the model of the specimen composed by 4×12 cells and two squared heads with the side of 20 mm is illustrated. The heads are realized for the clamping of the specimens on the tensile test machine. The nominal dimensions of the entire specimen are $100 \times 20.80 \times 4.80$ mm^3.

2.2 3D printing phase

Once the specimen realized, the model is exported on the stereolithography (STL) format for the 3D printing phase. A same STL file was used for both the 3D printer: Zortrax M200 (Zortrax©, Poland) for the ABS material and MarkTwo (Markforged Inc., USA) for the Onyx. To obtain a part with same characteristics, it was necessary uniform the main 3D printing parameters on the slicer software. Few parameters can be varied on the respective slicer software (Z-Suite and Eiger, respectively). For the replication of the 3D-printed part, the printing parameters are reported in Table 1. The building plate of the ABS 3D printer is automatically heated, once the print is launched, instead the Onyx 3D printer is not equipped with a heating building plate.

The print of each part in ABS and Onyx required 2 h and 21 min, although they have different slice heights, the build time is the same because only Zortrax (ABS material) builds 6 layers of interface support (raft). In MarkTwo, the raft was not necessary. Three replications for each material were realized. To evaluate the feasibility of printing of this kind of structure, using a precision caliber, the three main dimensions of length, width and thickness were measured.

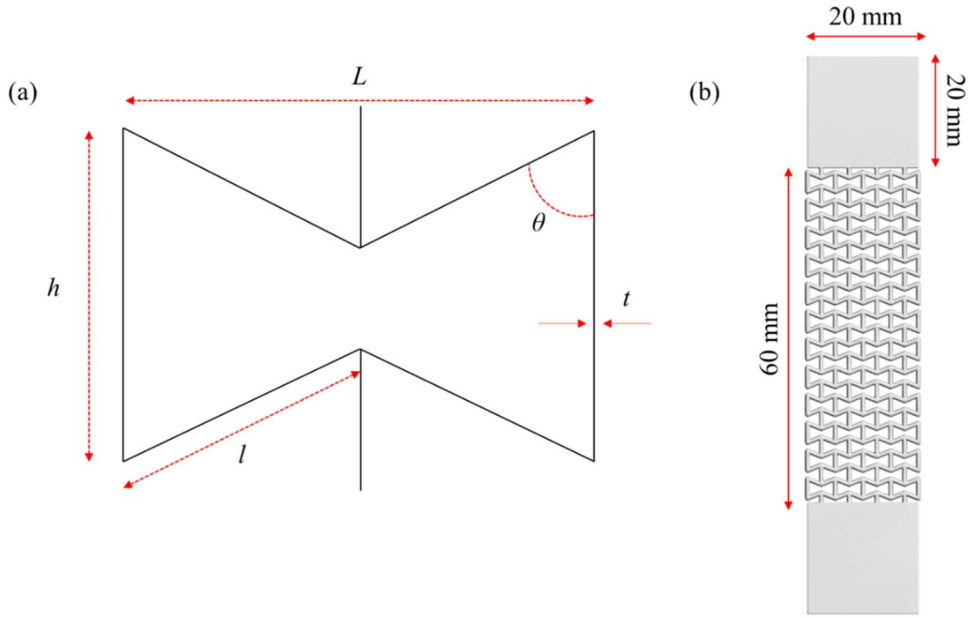

Fig. 1 **a** Design parameters of the re-entrant honeycomb cell. **b** Specimen used for the characterization

Table 1 Printing parameters for both materials

Material	Nozzle temperature (°C)	Nozzle diameter (mm)	Layer height (mm)	Infill density (%)	Printing direction	Heated build plate
ABS	235	0.40	0.09	100	XY	Yes
Onyx	275	0.40	0.10	100	XY	No

2.3 Tensile testing and DIC

The tensile testing was performed using the universal testing machine, Instron 4458 (load cell of 200 kN) and the DIC system ARAMIS 3D for measuring the strains on the entire structure with an acquisition frequency of 1 Hz. Before each test, the specimens were prepared for the deformation acquisition. Specifically, black specimens (Onyx ones) were sprayed with a random white speckle pattern, instead the gray specimens (ABS ones) were first tinted with a white matte layer background to avoid reflection and then sprayed with a random black speckle pattern. A crosshead speed of 5 mm/min was selected for the tensile test according to the standard ISO 527-1:2019 "plastics—Determination of tensile properties—part 1: general principles".

The Poisson's ratio was analyzed considering three lines in three different areas of structure (near the mobile grip, in the middle of the specimen and near the fixed grip) and a single line in the middle of the specimen for both materials. The three lines were drawn in the transversal direction (*X*-axis) and the single line in the axial direction (*Y*-axis).

For each line, using the DIC system, the variation of their length was calculated. Consequently, the transversal and axial strains were derived according to the Eqs. 1 and 2. The Poisson's ratio for each line (ν_j) was calculated using the Eq. 3

$$\varepsilon_{\text{transversal},j} = \frac{l_{i,j} - l_{0,j}}{l_{0,j}}, \tag{1}$$

$$\varepsilon_{\text{axial}} = \frac{l_i - l_0}{l_0}, \tag{2}$$

$$\nu_j = -\frac{\varepsilon_{\text{transversal},j}}{\varepsilon_{\text{axial}}}. \tag{3}$$

The $l_{i,j}$ is the length at time step *i*th of the number line *j*, while $l_{0,j}$ is the initial length of the number line *j*. The variable $\varepsilon_{\text{transversal},j}$ is the transversal strain of the number line *j*, while $\varepsilon_{\text{axial}}$ is the axial strain.

In Fig. 2, an example of the analysis method for studying ν value is reported.

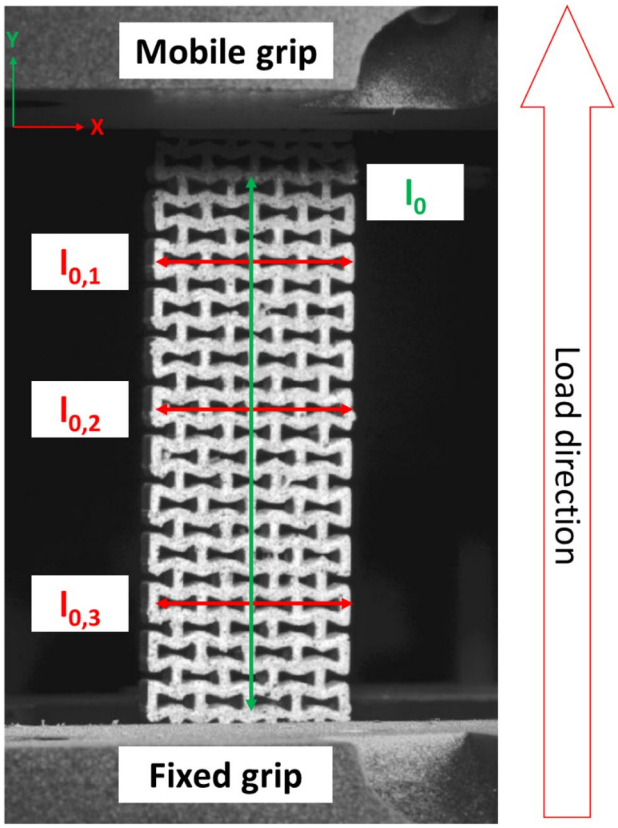

Fig. 2 Example of lines considered for the measure of Poisson's ratio

3 Results and discussion

3.1 Preliminary results of 3D-printed cell

Preliminary tests showed how using a *L* lower than 5 mm caused several defects on the 3D-printed cells for both materials. In Fig. 3a, b, using a *L* equal to 3.5 mm, it can be observed these defects such as many re-melted zones, areas with different geometry compared to the designed one, blobs and lack of adhesion between the wall lines. These manufacturing defects observe for small features confirmed what reported in [17].

As a consequence, as reported in Sect. 2.1, *L* equal to 5 mm was set for the specimens adopted for these experiments.

3.2 Dimensional analysis

The dimensional analysis of each specimen was carried out by measuring their weight, length, width and thickness. Three measurements were taken for each quantity. The dimensions of the specimens realized in ABS and Onyx are reported in Table 2.

Figure 4a shows the specimens 3D printed with the two different materials. The cells reported in Fig. 4b–c confirmed the feasibility of manufacturing these types of structures using the MEX technology. The structure in ABS reported an excess of material extruded on the struts and re-entrant angle. Some re-melted zones were observed due to the nozzle passage for the realization of the layer. Instead, the

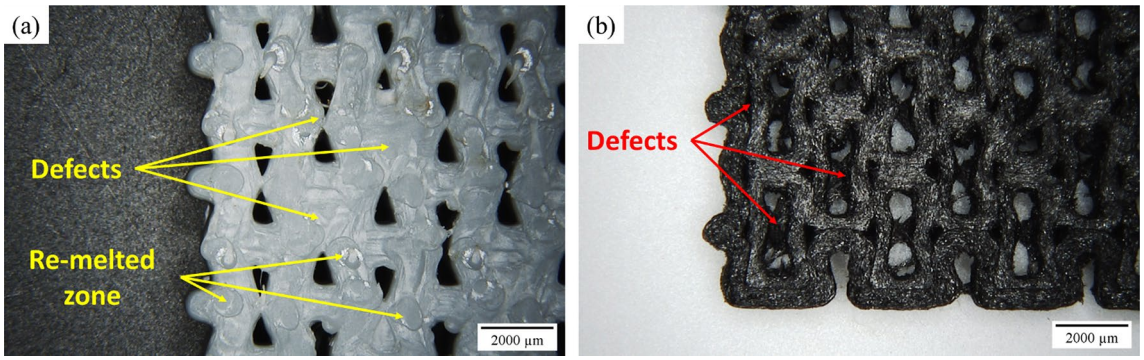

Fig. 3 Defects of preliminary 3D-printed cell for **a** ABS and **b** Onyx

Table 2 Dimensional values. The weight was evaluated using a precision balance ($d = 0.005$ g)

Material	Weight (g)	Length (mm)	Width (mm)	Thickness (mm)
ABS	7.36 ± 0.02	99.69 ± 0.02	20.81 ± 0.02	4.85 ± 0.03
Onyx	7.22 ± 0.06	99.35 ± 0.04	20.59 ± 0.02	4.66 ± 0.02

structure realized in Onyx showed a better surface quality with no significant defects.

According to the work of Wan et al. [25], it is possible to define the relative density (R) of the auxetic structure using the geometrical aspect (t, h, l and θ) of the cell (Eq. 4). Using an optical microscope and an image analysis software such as ImageJ, it was possible define an approximate measure of the geometrical aspects of cell required by the formula..

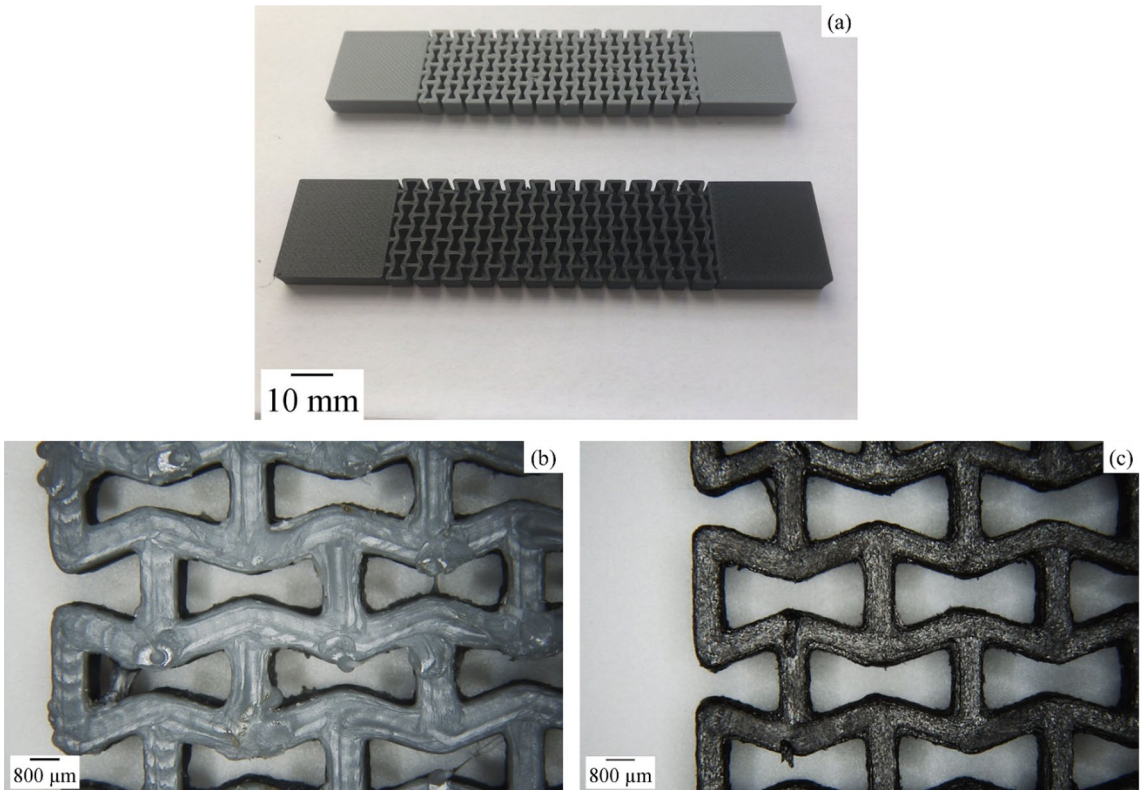

Fig. 4 **a** Auxetic specimens realized in ABS (gray one) and Onyx (black one). Focus using an optical microscope on cell realized in **b** ABS and **c** Onyx

$$R = \frac{\frac{t}{l} \times (\frac{h}{l} + 2)}{2 \times \cos\theta \times (\frac{h}{l} - \sin\theta)}. \quad (4)$$

Considering the nominal value of h, l, t and θ defined in this work, the R estimated was 38%. After the image analysis, the R estimated for ABS and Onyx were, respectively, 43% and 39%. The increment of R for ABS was due to an excess of extruded material during the 3D printing phase. This is confirmed by the mean measured value of the strut thickness was 1.06 mm, about the 33% more compared to the nominal value (0.80 mm) and 20% compared to the thickness of Onyx strut (0.88 mm).

3.3 Evaluation of Poisson's ratio

Tensile tests on the two investigated materials showed a greater elongation at break ($A\%$) for Onyx; instead, their ultimate tensile strength (UTS) was comparable; therefore, Fig. 5a shows an example of strain/stress curves for ABS and Onyx where the UTS are 5.35 MPa and 5.45 MPa, respectively. The mean value of $A\%$ for Onyx was approximately 24% and for ABS about 5%. Less relevant the difference on the average UTS, that was equal to 5.51 MPa and 4.51 MPa for Onyx and ABS, respectively.

Figure 5b shows, as an example, the broken specimens for the investigated materials. In each replication, a central fracture was observed for ABS, while for Onyx the fracture was localized near to the fixed grip.

To observe the auxetic behavior in both cases, the capability of DIC system was exploited. Three transversal lines near the mobile grip (line 1), on the middle (line 2) and near the fixed grip (line 3) were defined on the specimens using ARAMIS software. First, the transversal strain was evaluated over the time for each material and different regions by adopting the Eq. 1. The derived trend was observed, for all replications, in Fig. 6a for ABS and Fig. 6b for Onyx.

From Fig. 6a**,** the transversal strain of ABS specimen tends first to decrease slightly and then to increase; therefore, the auxetic behavior occurs from the moment the $\varepsilon_{\text{transversal}}$

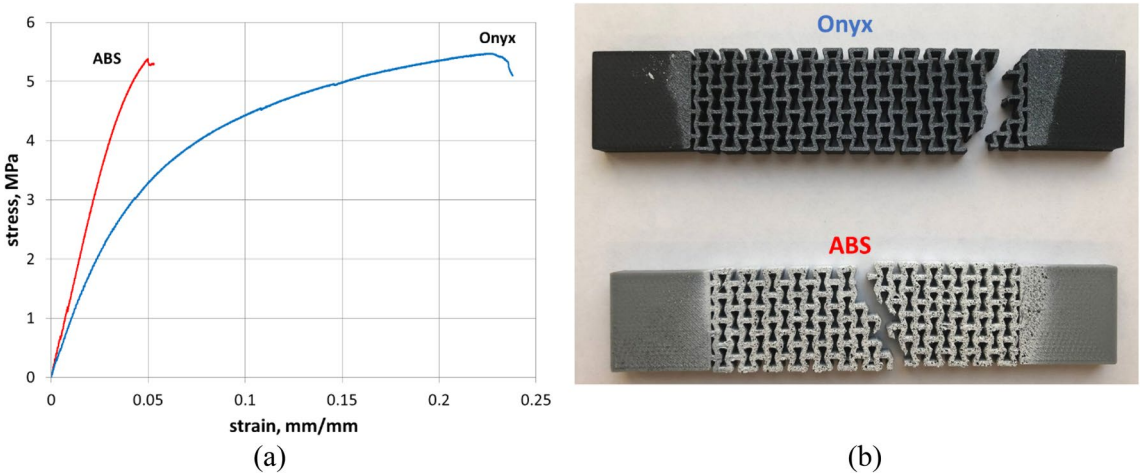

Fig. 5 **a** Example of stress vs strain curve of ABS and Onyx; **b** ABS and Onyx broken specimens

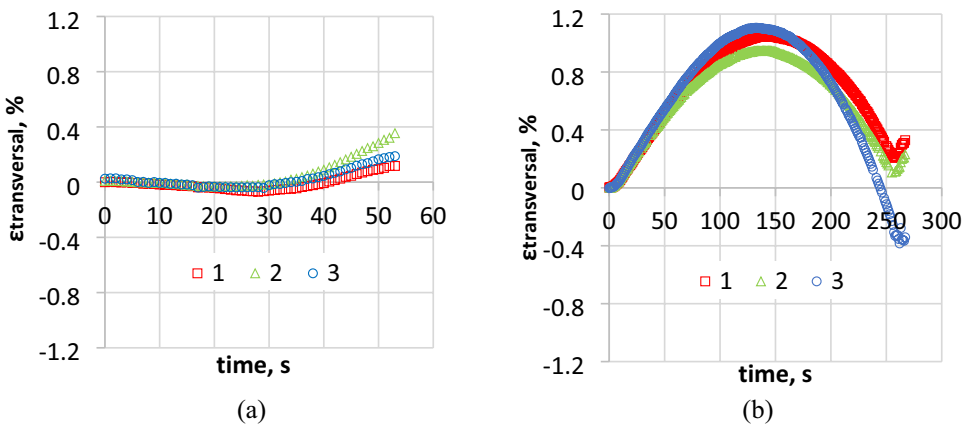

Fig. 6 Transversal strain measured next to the mobile grip 1), middle 2) and fixed grip 3) for **a** ABS **b** Onyx

start to increase. For Onyx specimen (Fig. 6b), instead, tends to increase and then to decrease. For this material, the auxetic behavior can be observed already from the beginning of the tensile test.

The maximum percentage increase of strain in *X*-direction, in the moment that the materials exhibit an auxetic behavior, was recorded for ABS and Onyx in correspondence of the area where the fracture occurs (line 2 for ABS and line 3 for Onyx). These values of transversal strain approached to on average 0.4% for ABS and an average value of 1.1% for Onyx. Considering the strain in *Y*-direction, a linear trend was observed for both materials. The axial strain increases up to about 6% for ABS and about 35% for Onyx.

To highlight that the auxetic behavior begins when the transversal strain increase, the graphs in Fig. 7a for ABS and Fig. 7b for Onyx were plotted. Here, both the Poisson's ratio and $\varepsilon_{transversal}$ as a function of ε_{axial} are shown. As expected, when the transversal strain assumes positive values, the Poisson's ratio exhibits negative values. By comparing the Poisson's ratio for both material, Onyx kept an NPR approximately for the entire test ($0 < \varepsilon_{axial} < 30\%$), while tends to change from negative to positive at the end of the tensile test, as confirmed in previous works on 2D re-entrant honeycomb [13, 25, 30]. On the other hand, ABS presented an NPR in the range of axial strain between 3 and 6%.

The Poisson's ratio was evaluated in correspondence of the three considered lines as a function of the axial strain. The results were reported in Fig. 8a for ABS specimen and Fig. 8b Onyx specimens.

With the aim to confirm that the different trend of NPR for both materials did not affect by the printing resolution, other specimens with greater size were printed and the relative density was kept constant compared to the small specimens (39% and 43% for Onyx and ABS, respectively). Figure 9 compares the small and large broken specimens. It can be observed that the breakage occurs always in the same way for all specimens independently from its size. Moreover, the DIC data demonstrated that the NPR trend does not change with the specimens dimensions both for Onyx and ABS. An absence of printing defects was observed for the large specimens compared to the small ones reported in Fig. 4a. In the large specimens, the mean value (1.58 mm) of the strut thickness was 1.25% lower than nominal value (e.g., 1.60 mm) for Onyx, instead for the ABS, it is more than 16.9% (1.87 mm). The difference in the strut thickness was about the half of what found on the small specimen (33%).

For the structure in ABS, the mean value of NPR ranges between −0.06 and −0.02; instead, Onyx structure reported a mean value of NPR between −0.13 and 0. The trends reported, on the different investigated regions of ABS, are

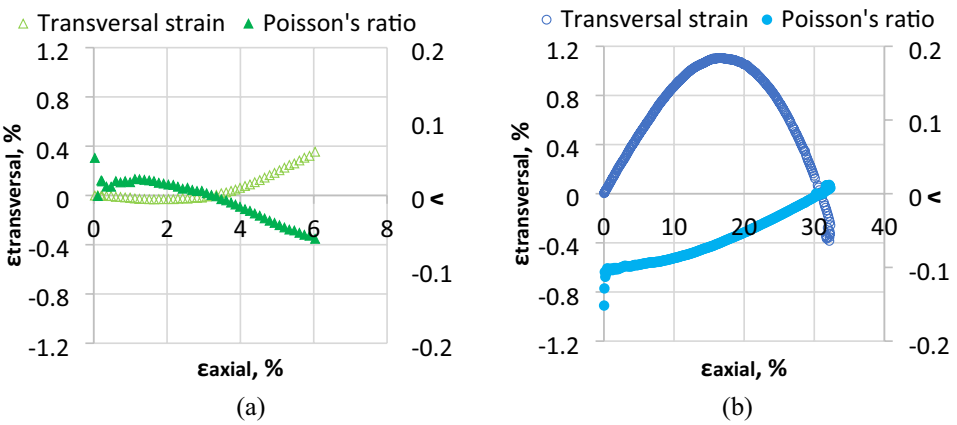

Fig. 7 Poisson's ratio and εtransversal as a function of ε_{axial} for **a** ABS and **b** Onyx

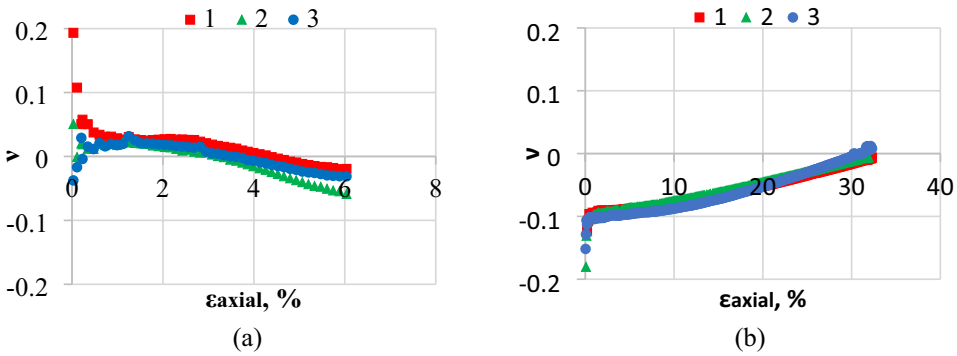

Fig. 8 Trend of Poisson's ratio vs ε_{axial} for **a** ABS, **b** Onyx along 1, 2, 3 lines

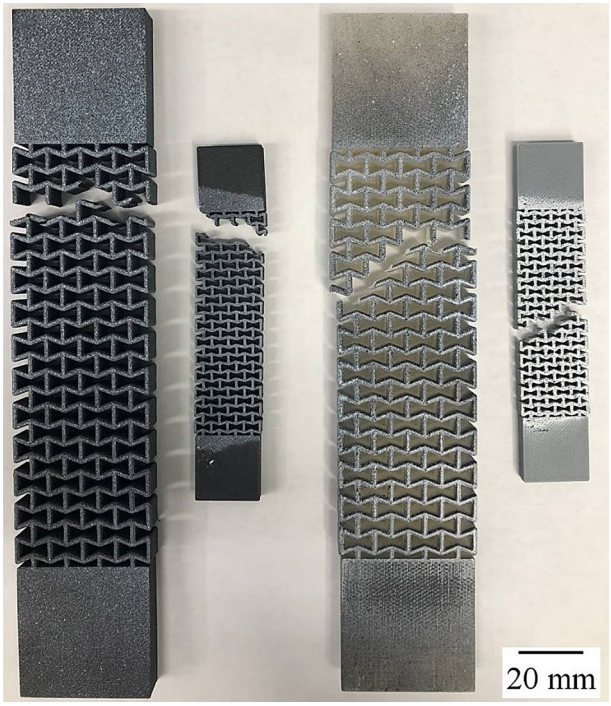

Fig. 9 Comparison of specimens large and small

closed to that reported by Riva et al. [23]. In the present work is confirmed how the structure made in ABS tends to lower values of Poisson's ratio increasing the axial strain. The Onyx structures follow the same behavior as those shown by Meeusen et al. [13] on TPU and Ling et al. [31] on Nylon. How Fig. 8b shows, the negative values of ν are maintained up to a certain value of strain, then the structure loses its auxeticity up to the break. Therefore, the Onyx could be suitable for personal protective equipment and automotive applications thanks both to its capability to keep an auxetic behavior at high strain and a good stiffness (2.4 GPa of tensile modulus as reported technical data sheet). TPU structures showed a similar trend of NPR at high strain, as recorded in Onyx but a low stiffness equal to 0.25 GPa. Confirming the results already explained for Fig. 6, the greater values of negative Poisson's ratio were recorded near the line corresponding to the breaking point (Fig. 8a, b).

4 Conclusions

The results described in the present work allowed to provide the follow considerations:

- The geometrical aspects of the structure (t, h, l and θ) confirmed the auxetic behavior for ABS and Onyx material.
- Tensile tests allowed to observe a greater ductility of structures printed with Onyx ($\simeq 25\%$ of A%) compared to the ABS ($\simeq 5\%$ of A%) but not relevant differences for the UTS.
- The material has a great influence on the auxetic behavior of the same structure. In fact, the Poisson's ratio of ABS tends to be negative at the end of the tensile test for an axial strain between 3 and 6%. Instead, Onyx exhibits an NPR for the whole tensile test. Material affects the trend of Poisson's ratio and its value. In fact, for ABS $-0.06 < \nu < -0.02$, while for Onyx $-0.13 < \nu < 0$.
- The Onyx structures follow the same behavior of those in TPU, with different scale of values, but Onyx material has a tensile strength 960% higher than TPU. Therefore, auxetic structures made with CFRP could be used in applications where it is important to have objects capable of absorbing energy before breaking.
- The choice of the material and the geometrical aspects is strongly influenced by the application field and by the manufacturing technology. The manufacturing defects in the auxetic structures that can rise for a thinner strut or too small features are related to the technologic limits of the process. Increasing the size of the cell, a substantial decrease in printing defects was found.
- New studies will be carried out on the realization of auxetic structures with three-dimensional development that can only be realized with AM technologies. New engineered materials and other AM technology could be considered for the characterization of these NPR shapes according to the application field.

Acknowledgements This research work was undertaken in the context of the project PON "R&I" 2014-2020 ARS01_00806 "Soluzioni Innovative per la qualità e la sostenibilità dei processi di ADDitive manufacturing".

Funding Open access funding provided by Politecnico di Bari within the CRUI-CARE Agreement. This work was supported by the Italian Ministry of Education, University and Research under the Programme "Department of Excellence" Legge 232/2016 (Grant No. CUP—D94I18000260001).

Data availability The experimental data are available under request.

Declarations

Conflict of interest The authors declare that they have no conflict of interest.

References

1. Joseph A, Mahesh V, Harursampath D (2021) On the application of additive manufacturing methods for auxetic structures: a review. Adv Manuf 9:342–368. https://doi.org/10.1007/s40436-021-00357-y
2. Evans KE, Nkansah MA, Hutchinson IJ et al (1991) Molecular network design. Nature 353:10065
3. Carneiro VH, Puga H (2018) Axisymmetric auxetics. Compos Struct 204:438–444. https://doi.org/10.1016/j.compstruct.2018.07.116
4. Lakes RS (1986) Foam structures with a negative Poisson' s ratio. Science (80-) 435:1038–1040
5. Lakes RS (1993) Design considerations for materials with negative poisson's ratios. J Mech Des Trans ASME 115:696–700. https://doi.org/10.1115/1.2919256
6. Lakes RS, Elms K (1993) Indentability of conventional and negative Poisson's ratio foams. J Compos Mater 27:1193–1202. https://doi.org/10.1177/002199839302701203
7. Scarpa F, Ciffo LG, Yates JR (2004) Dynamic properties of high structural integrity auxetic open cell foam. Smart Mater Struct 13:49–56. https://doi.org/10.1088/0964-1726/13/1/006
8. Keskar NR, Chelikowsky JR (1992) Negative Poisson ratios in crystalline SiO_2 from first-principles calculations. Nature 358:222–224. https://doi.org/10.1038/358222a0
9. Yeganeh-Haeri A, Weidner DJ, Parise JB (1992) Elasticity of α-cristobalite: a silicon dioxide with a negative Poisson's ratio. Science (80-) 257:650–652. https://doi.org/10.1126/science.257.5070.650
10. Williams JL, Lewis JL (1982) Properties and an anisotropic model of cancellous bone from the proximal tibial epiphysis. J Biomech Eng 104:50–56. https://doi.org/10.1115/1.3138303
11. Galantucci LM, Guerra MG, Dassisti M et al (2019) Additive manufacturing: new trends in the 4th industrial revolution. Springer International Publishing, Cham. https://doi.org/10.1007/978-3-030-18180-2_12
12. Berrocal L, Fernández R, González S et al (2019) Topology optimization and additive manufacturing for aerospace components. Prog Addit Manuf 4:83–95. https://doi.org/10.1007/s40964-018-0061-3
13. Meeusen L, Candidori S, Micoli LL et al (2022) Auxetic structures used in kinesiology tapes can improve form—fitting and personalization. Sci Rep. https://doi.org/10.1038/s41598-022-17688-w
14. Li Z, Wang X, Ma L et al (2022) Study on the mechanical properties of CFRP composite auxetic structures consist of corrugated sheets and tubes. Compos Struct. https://doi.org/10.1016/j.compstruct.2022.115655
15. Takaichi A, Kajima Y, Kittikundecha N et al (2020) Effect of heat treatment on the anisotropic microstructural and mechanical properties of Co–Cr–Mo alloys produced by selective laser melting. J Mech Behav Biomed Mater 102:103496. https://doi.org/10.1016/j.jmbbm.2019.103496
16. Suwanpreecha C, Manonukul A (2022) On the build orientation effect in as-printed and as-sintered bending properties of 17–4PH alloy fabricated by metal fused filament fabrication. Rapid Prototyp J 28:1076–1085. https://doi.org/10.1108/RPJ-07-2021-0174
17. Zamani MH, Heidari-Rarani M, Torabi K (2022) Optimal design of a novel graded auxetic honeycomb core for sandwich beams under bending using digital image correlation (DIC). Compos Struct 286:115310. https://doi.org/10.1016/j.compstruct.2022.115310
18. Pellegrini A, Palmieri ME, Guerra MG (2022) Evaluation of anisotropic mechanical behaviour of 316L parts realized by metal fused filament fabrication using digital image correlation. Int J Adv Manuf Technol. https://doi.org/10.1007/s00170-022-09303-z
19. Yang L, Cormier D, West H et al (2012) Non-stochastic Ti-6Al-4V foam structures with negative Poisson's ratio. Mater Sci Eng A 558:579–585. https://doi.org/10.1016/j.msea.2012.08.053
20. Mizzi L, Azzopardi KM, Attard D et al (2015) Auxetic metamaterials exhibiting giant negative Poisson's ratios. Phys Status Solidi Rapid Res Lett 9:425–430. https://doi.org/10.1002/pssr.201510178
21. Liu H, Kollosche M, Yan J et al (2020) Numerical investigation of auxetic textured soft strain gauge for monitoring animal skin. Sensors (Switzerland) 20:1–17. https://doi.org/10.3390/s20154185
22. Qiao J, Chen CQ (2015) Analyses on the in-plane impact resistance of auxetic double arrowhead honeycombs. J Appl Mech 82:1–9. https://doi.org/10.1115/1.4030007
23. Riva L, Ginestra PS, Pandini S et al (2022) Production and characterization of the Poisson's ratio of cellular structured metamaterials by additive manufacturing. Proc CIRP 110:378–382. https://doi.org/10.1016/j.procir.2022.06.067
24. Almahri S, Schneider J, Schiffer A et al (2022) Piezoresistive sensing performance of multifunctional MWCNT/HDPE auxetic structures enabled by additive manufacturing. Polym Test 114:107687. https://doi.org/10.1016/j.polymertesting.2022.107687
25. Wan H, Ohtaki H, Kotosaka S et al (2004) A study of negative Poisson's ratios in auxetic honeycombs based on a large deflection model. Eur J Mech A/Solids 23:95–106. https://doi.org/10.1016/j.euromechsol.2003.10.006
26. Fu MH, Bin ZB, Li WH (2017) A novel chiral three-dimensional material with negative Poisson's ratio and the equivalent elastic parameters. Compos Struct 176:442–448. https://doi.org/10.1016/j.compstruct.2017.05.027
27. Wang XT, Wang B, Li XW et al (2017) Mechanical properties of 3D re-entrant auxetic cellular structures. Int J Mech Sci 131–132:396–407. https://doi.org/10.1016/j.ijmecsci.2017.05.048
28. Wang XT, Chen YL, Ma L (2018) The manufacture and characterization of composite three-dimensional re-entrant auxetic cellular structures made from carbon fiber reinforced polymer. J Compos Mater 52:3265–3273. https://doi.org/10.1177/0021998318764021
29. Bronder S, Adorna M, Fíla T et al (2021) Hybrid auxetic structures: structural optimization and mechanical characterization. Adv Eng Mater. https://doi.org/10.1002/adem.202001393
30. Zhang J, Lu G, Wang Z et al (2018) Large deformation of an auxetic structure in tension: Experiments and finite element analysis. Compos Struct 184:92–101. https://doi.org/10.1016/j.compstruct.2017.09.076
31. Ling B, Wei K, Wang Z et al (2020) Experimentally program large magnitude of Poisson's ratio in additively manufactured mechanical metamaterials. Int J Mech Sci. https://doi.org/10.1016/j.ijmecsci.2020.105466
32. Stratasys (2022) ABS-M30 FDM thermoplastic filament. https://www.stratasys.com/en/materials/materials-catalog/fdm-materials/abs-m30/
33. Markforged Inc. (2021) Material datasheet composites. http://static.markforged.com/downloads/composites-data-sheet.pdf